Modeling Operational Variability for Robust Multidisciplinary Design Optimization

Nicolas Peteilh, Marcel Mongeau, Christian Bes, Mélanie Conderolle-Lestremau, Thierry Druot

HAL Id: hal-01534843
https://enac.hal.science/hal-01534843

Submitted on 28 Jun 2017

Modeling operational variability for aircraft robust Multidisciplinary Design Optimization

N. Peteilh* , M. Mongeau†

ENAC, Université de Toulouse, France

C. Bes‡

Université Paul Sabatier (UPS), Université de Toulouse, France

M. Conderolle-Lestremeau§ , T. Druot¶

Airbus, Toulouse, France

The aim of this paper is to model and propagate operational uncertainties in view of its integration in a multidisciplinary optimization methodology for aircraft robust design. From databases relative to one specific type of long-range airplane, we analyze the variations of four flight parameters (altitude, speed, temperature and range), and build the associated statistical distributions. Then, using an uncertainty propagation methodology, we identify the distribution of operational costs.

I.   Introduction

The need to reduce the environmental impact of air transportation is today widely recognized. The Advisory Council for Aviation Research and innovation in Europe (ACARE) has identified energy supplies and the protection of the environment as key challenges in its Strategic Research and Innovation Agenda[1](SRIA). Airplane design is an important mean to meet the sustainable development requirements and, considering the development of the civil aviation sector, even a few percentages gained on fuel consumption have a strong impact on the environmental footprint of air transportation. In the last decades, manufacturers have largely improved airplane design using optimization methodologies. Today, one of the ways to achieve further significant improvements is to consider the interaction between the airplane and the other air transport system stakeholders such as airlines, airports, the passengers, the air traffic management, etc. This paper contributes to the quantification of the interactions between a manufacturer nominal aircraft design and its operational use by airlines.

Today, the design of a transport airplane starts with the definition of a set of requirements, which includes the description of a typical mission representing the anticipated future airplane operations. During the design phases, from the conceptual to the detailed designs, the airplane overall design is optimized with respect to this specific mission. Nevertheless, when it enters into service a few years later, it is operated by the airlines on their specific networks, according to the timetables and meeting the airlines' operational needs.

In practice, the missions the airplane has to fly greatly differs from the nominal mission for which it was optimized. In addition, the airplane has to face several types of operational variability, related for instance to temperature, altitude, range, payload, or speed. These variabilities are due to operational parameters that range from the airlines routes, on-board services, flight load factor, weather conditions (wind, temperatures, and atmospheric pressure), or even to the air navigation service activities. As a consequence, an airplane is hardly ever used for the original mission for which it was initially sized and optimized. Therefore, this may have a high impact on the operational costs.

---

*PhD Student, Optim research group, 7 avenue Edouard Belin, CS 54005, 31055 Toulouse cedex 4, and AIAA Member

†Professor, Optim research group, 7 avenue Edouard Belin, CS 54005, 31055 Toulouse cedex 4.

‡Professor, MS2M, Espace Clément Ader, 3 rue Caroline Aigle, 31400 Toulouse, and AIAA Senior Member.

§Apprentice engineer, 316 route de Bayonne, 31300 Toulouse.

¶Senior Engineer, 316 route de Bayonne, 31300 Toulouse.

American Institute of Aeronautics and Astronautics

The aim of this paper is to model and propagate operational uncertainties in view of its integration in a multidisciplinary-optimization tool for robust design. The paper is organized as follows. In the first section, we make a first analysis from databases that shows the high impact of range variability on costs. Section 2 provides histograms issued from another database that reflects the variability of the main flight parameters. Section 3 deals with the identification of the statistical models underlying these histograms. Section 4 introduces the overall airplane conceptual design model proposed. The last section is dedicated to the propagation of the statistical distributions of the flight parameters through the conceptual design models. More precisely, we estimate the statistical distribution of operational costs resulting from these input uncertainties.

II.   Preliminary study

The first step of the analysis is to assess whether the different kinds of variability would impact the cost per passenger and per nautical mile of a long-range airplane. Based on the OAG database,[2] a first analysis is carried out to confirm the large variety of ranges, and then to assess operational costs. The flights performed by long-range type airplanes such as A330, A340, A350, A380, B747, B777, and B787 are considered over a period of one year (2014), representing a total of 2,300,000 flights. The histogram of their range was plotted and analyzed as a whole and in more details for 22 airlines. The graphs presented in Figure 1 show the distributions (number of flights per range) obtained. The first graph shows that the long-range airplanes are used on a large scale of mission ranges, with a surprisingly-high peak of short-range flights. The three other histograms reveal different operational uses by the airlines. Airline 1 uses its long-range airplanes for a large variety of ranges, while Airline 5 operates them mainly on long-range flights, and Airline 10 flies mainly on short-range flights.
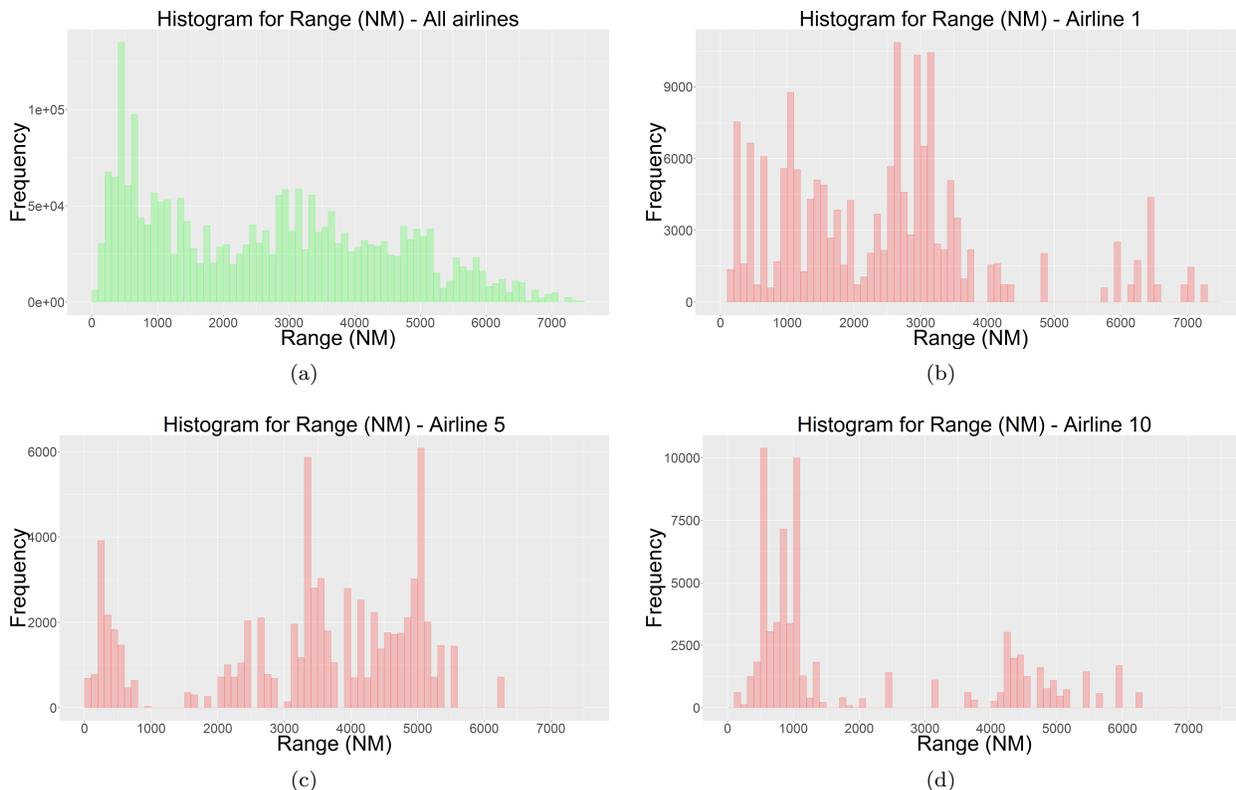
Figure 1. **Distributions (number of flights per range) obtained for all the airlines together (a), and for 3 of them exhibiting different behaviors: Airline 1 (b), Airline 5 (c) and Airline 10 (d).**

Based on these distributions, an evaluation of the cost per passenger and per nautical mile is then conducted for one specific long-range airplane type over a period of one year (2013) and for 19 airlines. For confidentiality reasons, a specific mission is chosen as a reference. Its range is 4000 NM. It corresponds to

American Institute of Aeronautics and Astronautics

the average mission used in the design process. All the costs are presented with respect to the cost of this reference mission. It is assumed that each flight carries the same number of passengers.

The results presented in Figure 2 show the cost per passenger and nautical mile as a function of the range. It is the Cash Operating Cost (COC) that includes costs related to the flight cycle, such as the maintenance or the airport taxes. This explains the high increase of costs for the short-range flights.
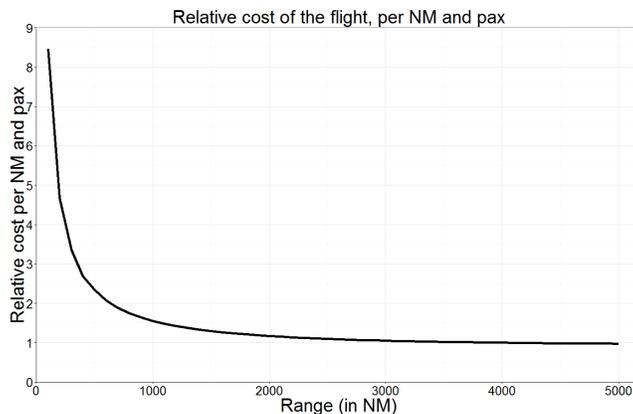

Figure 2. Average cost per passenger and per nautical miles as a function of range

Knowing the range distribution for each 19 airlines over a period of one year, the average cost is calculated and presented in Figure 3. The left-hand side part of the graph shows the average cost for each airline, and the right-hand side part displays an the histogram of the extra cast incurred. All the costs are higher that the reference one. It is concluded that the variability on the range impacts the average costs for the airlines in a negative way.
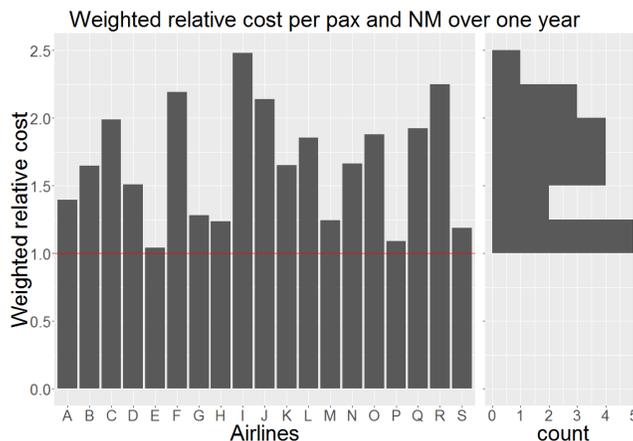

Figure 3. Average costs per passenger and per nautical miles for the studied airlines. The left-hand side part shows the cost for each airline (designated by a letter), and the right-hand side part presents the distribution of the extra costs.

Based on this first result, we further investigate the effect of variability on the costs.

III. Flight-parameter variability

These results prompt us to broaden the study and to study in more detail the four main flight parameters (temperature, speed, altitude and range) concerning one specific type of long-range airplane over a period

American Institute of Aeronautics and Astronautics

of twenty years.

These four parameters play a key role in the design phase as they affect the quantity of fuel necessary to fly the mission. The way they impact the quantity of fuel burnt during one flight (called block fuel) can be described using the Breguet-Leduc equation of the specific range R_S:

$$R_S = \frac{L/D \ \ V}{m \ \ g \ \ TSFC} \tag{1}$$

where V is the airspeed, $TSFC$ stands for the Thrust Specific Fuel Consumption, L/D for the Lift-to-Drag ratio, and g is the gravitational constant ($= 9.81 m/s^2$). The specific range can be integrated over the whole flight, and assuming constant airspeed, thrust specific fuel consumption, and lift-to-drag ratio as well as ascending cruise trajectory. The result is the integral expression of Breguet-Leduc equation:
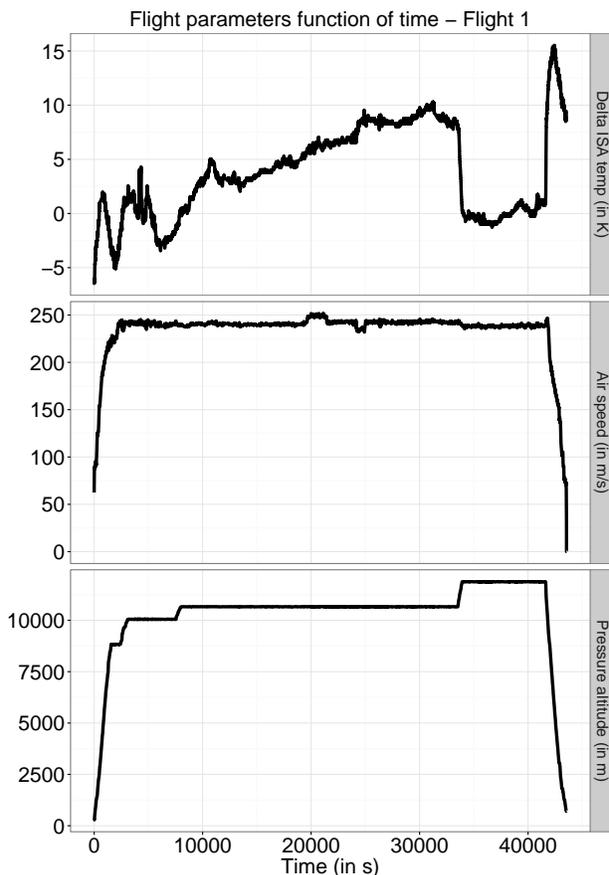
$$\frac{m_{fuel}}{MWE + OIW + Payload + Fuel_{reserve}} = \exp\left(\frac{g \ Range \ TSFC}{V \ L/D}\right) - 1 \tag{2}$$

where MWE stands for Manufacturer Weight Empty and OIW for Operating Items Weight, m_{fuel} is the quantity of fuel burnt during the flight and the $Fuel_{reserve}$ includes all regulatory fuel reserves. The airspeed and the range are directly related to the mission calculation. The temperature and the cruise altitude influence both the engine $TSFC$ and the airplane aerodynamic efficiency L/D.

The choice of the airplane type is made considering the availability of operational data. The in-service information is found in the database created by the European project MOZAIC.[3] It includes the flight history of four airplanes over a period of 20 years, for a total of 31,000 flights. All trajectory, time and meteorological data are then available. For each flight, one data set is provided every four seconds.

The amount of information to be managed is very high and care must be taken when processing this information. Indeed, as the intent of this work is to represent the operational variability using density functions and models, it must be ensured that all the elementary events used for estimating the statistical distribution are randomly drawn. As we focus on four specific airplanes over a period of 20 years, the hypothesis of random draw of the data observed cannot be fully validated. However, for the purpose of this study, we make this assumption by considering that the sample is representative. The values used to represent the airspeed, flight altitude and temperature variabilities are the average values during the cruise. The range distribution presented is the air range. For the special case of the temperature, the value considered is the difference between the measured in-flight temperature and the International Standard Atmosphere (ISA) temperature at the measured flight pressure altitude. This is designated by the "delta ISA temperature" or simply by "temperature" from now on.

Figure 4. Example of the evolution of the flight parameters (delta ISA temperature, airspeed and pressure altitude) along one particular flight

Figure 4 shows an example of the evolution of the flight parameters along one particular long-range flight.

American Institute of Aeronautics and Astronautics

For each flight, the cruise phase is therefore isolated, and average values are then calculated. The graphs presented in Figure 5 show the histograms obtained for the four parameters analyzed (air range, cruise altitude, airspeed, and temperature).

The distributions related to air range and cruise altitude are less smooth than those for airspeed and temperature. Concerning cruise altitude, the correlation with the air traffic management is highlighted by the different peaks corresponding to specific flight levels. For air range, we find here a result consistent with the preliminary remarks made in Section II where the airline route network is a hard constraint for range. In addition, we can see here that the dispersion in the air range is not only visible at the level of the whole set of airlines but also at the level of this small sub-set of four airplanes. Moreover, the meteorological conditions have an impact, as the winds have an effect (either positive or negative) on the air range as well as the airlines choice of the ground route, and also the air space management by the air traffic management entities. Airspeed and temperature are smoother. This seems consistent with the fact that airplanes are optimized for flying at a specific Mach number or cost index, which anyway leads at the end to quite constant speeds (since altitude is close or above tropopause). The variability related to temperature appears in line with the meteorological conditions all around the year and all around the world because of seasons. As the time period observed covers many years and long-range airplanes often fly across a large panel of latitudes and during both day and night times, we understand that the probability of meeting a large range of temperatures is high.
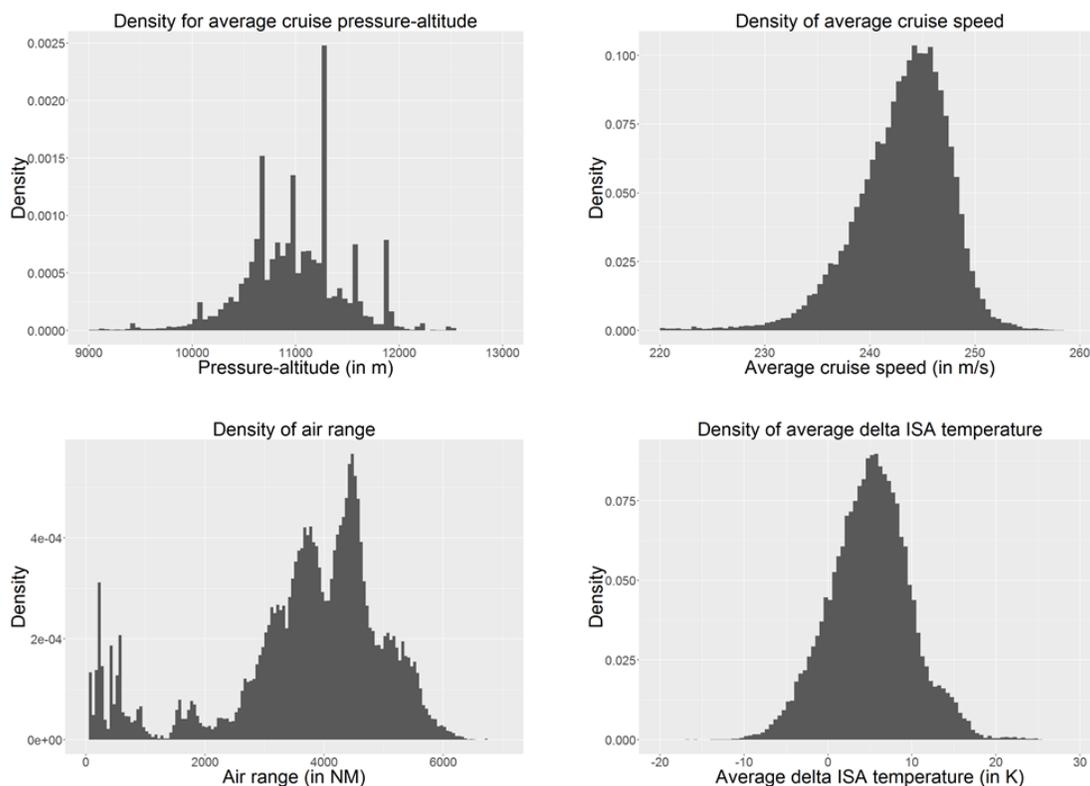
Figure 5. Flight parameters distributions

The next step of this analysis is to propose statistical models for the flight parameters variability observed.

IV. Statistical models of flight-parameter variability

The objective of this section is to model the various kinds of operational variability of flight parameters, based on the histograms obtained and showed in Figure 5. In order to propagate the uncertainty through the design model presented in Section V, we choose, when possible, to model the underlying statistical

American Institute of Aeronautics and Astronautics

distribution using the four-parameter beta distribution for its very interesting features: compact support, continuous, and encompassing several types of basic probability density functions. Another advantage of the beta distribution is that it allows the method of moment propagation to be used to reduce the calculation time compared to the Monte Carlo method.

The probability density function of the four-parameter beta distribution is given by:

$$D(x, a, b, p, q) = \begin{cases} \frac{(b-x)^{q-1}(x-a)^{p-1}}{\beta(p,q)(b-a)^{p+q-1}} & \text{if } a \leq x \leq b \\ 0 & \text{if } x < a \text{ or } b < x \end{cases} \tag{3}$$

where $\beta(p,q) = \frac{\Gamma(p)\Gamma(q)}{\Gamma(p+q)}$, and Γ is the gamma law.

The graph presented in Figure 6 illustrates different shapes that can be modeled using the four-parameter beta distribution. The values of a and b that control the interval covered by the distribution are fixed respectively to 0 and 1. The rows and columns are respectively related to the *skewness* and *kurtosis* coefficient of the distribution. For example, in Figure 6, the skewness is modified from one column to another and the asymmetry of the distribution moves from one side to the other. The kurtosis is modified from one line to the other and we can see the distribution to change from "flatter" to more "peaky". A comparison of these shapes with the flight parameter distributions in Figure 5 tends to show that the cruise speed and the delta ISA temperature can be represented by a beta distribution. However, this type of distribution seems not to be adequate for the pressure altitude and air range distribution displayed in Figure 5.
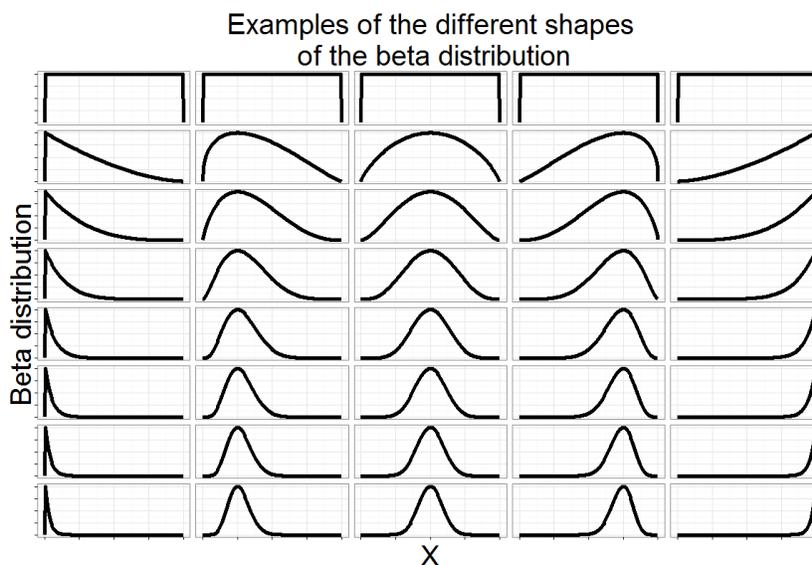

Figure 6. Examples of different shapes the beta probability density function can take.

In order to calculate the four parameters' values of the beta distribution, we use a least-square minimization method to fit each cumulative beta distribution function with the corresponding empirical distribution function. Although more adequate for the delta ISA temperature and the cruise speed, the calculation is made for the pressure altitude and the air range as well. The values obtained for the mean value and the four parameters of the beta distribution are presented in Table 1.

The graphs shown in Figure 7 represent the same distributions as Figure 5 together with the computed beta density functions (in red). As anticipated, the models fit adequately the delta ISA temperature and the cruise speed uncertainties but they appear not to match those related to air range and cruise altitude empirical distributions. For these two parameters, further analysis and other models will be considered but this is out of the scope of this paper.

American Institute of Aeronautics and Astronautics

Table 1. Estimations of the four parameters of the beta distribution using 2 methods.

	Delta ISA temperature (K)	Cruise airspeed (m/s)	Pressure altitude (m)	Air range (NM)
Mean	5.03	242.91	10991	3703
a	-34.15	210 [*]	9002 [†]	55.98
b	25.41	254.75	12531	6741
p	22.49	17.386	7.336	3.190
q	11.71	5.922	5.673	2.586

[*] To get a good matching, it was necessary to keep only the airspeed data above 210 m/s, which seems reasonable noting that 96% of the speeds are above 220 m/s.

[†] To get a better matching, it was necessary to keep only the altitude data above 9000 m, which seems reasonable because 95% of the pressure altitudes are above 9000 m.
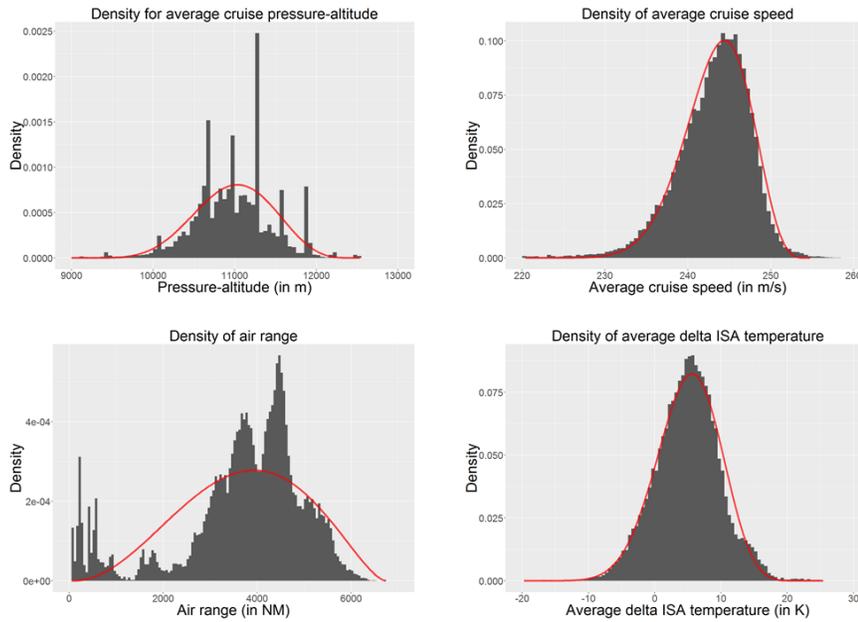
Figure 7. Flight parameters distributions and associated beta density functions.

V. Overall airplane-design model

This section first presents the computational process and its sequence of operations. Then, it describes the airplane used as reference for this application.

A. Computational process

The Overall Airplane-Design (OAD) process that we use is based on an Airbus aircraft toolbox called OC-CAM.[4,5] It is dedicated to research activity, and developed in Scilab.[6] The models used are empirical or semi-empirical and allow for fast time calculations. They are simple but realistic and involve all main physics such as geometry, weights, aerodynamics, low and high speed performances, route performances and costs. The aircraft is described by around 200 parameters.

The granularity chosen in the description of the process used for this analysis is presented in Figure 8 using an extended design structure matrix (XDSM)[7] representation. It aims at giving the reader a global overview of the process, considered as a multidisciplinary analysis. It starts with an MDA block that manages the input data and more precisely the Top Level Aircraft Requirements (TLARs). The sequence of operations

American Institute of Aeronautics and Astronautics

is as follows :

1. Initiate MDA process

2. Compute airplane geometry

3. Pass data and initiate mass-mission optimization loop

4. Compute masses

5. Compute mission

   (a) Compute high speed aerodynamics
   (b) Compute propulsion

6. Check for mass-mission loop convergence. If it has not converged, return to 4; otherwise, continue.

7. Compute performances

8. Compute Costs

The TLARs include the total number of passengers, the design range, the operational Mach number, the cruise altitude, the number of engines, the engine By-Pass-Ratio (BPR), and the aspect ratio.
Other input parameters useful for this study include the delta ISA temperature for cruise.

The geometry analysis computes a total of 36 parameters that describe the cabin and the fuselage, the wing, the horizontal and vertical tails, and the nacelles.
A specific emphasis has been put on the mass-mission loop which is at the core of the calculation. As described by J. Birman,[4] this loop is intended to compute the Maximum Take-Off Weight (MTOW) of the aircraft so that it matches both the structural strength and the range requirements. The initial operation is named "Masses" and its primary role is to compute, based on an initial guess of the design MTOW and Maximum Zero-Fuel Weight (MZFW), the main component mass breakdown and a classical set of design weights, including more particularly the Operating Weight Empty (OWE). It also returns the nominal payload and the maximum payload. The second step is to calculate, from an initial estimation of the block fuel and MTOW, the total fuel, range and Zero-Fuel Weight (ZFW), by using for instance the Breguet-Leduc equation shown in Eq. 2. This operation requires the computation of aerodynamic and propulsion parameters such as the lift-to-drag ratio or the thrust specific fuel consumption. The optimization loop will iterate until the following set of equation is solved:

$$
\begin{cases}
MTOW = OWE + NominalPayload + FuelTotal \\
MZFW = OWE + MaxPayload \\
DesignRange = Range
\end{cases}
\tag{4}
$$

Once the optimization process has converged, the operational and mission performances, such as the climb and cruise ceilings, the time-to-climb, the minimum climb path angle, the altitude of maximum specific air range, the take-off and landing distances, the landing speed, etc. are computed.
Finally the COC, the Direct Operating Cost (DOC) and the Recurring Costs (RC) are calculated.
The performances and costs are then output of the process, as well as the MTOW and the MZFW.

B.   Reference airplane

The operational variabilities that have been observed and modeled in the previous sections correspond to a specific long-range airplane type. In order to propagate the uncertainties and evaluate the impact on costs and the MTOW, we choose a reference airplane having the characteristics presented in Table 2 and Table 3.

The geometry of the reference airplane is presented in the 3-view drawing of Figure 9.

The presentation of the airplane design process and of the reference airplane is now finished. In the next section, we look at the impact of the uncertainties on the costs by propagating the uncertainties through the design process.

American Institute of Aeronautics and Astronautics

Table 2. Top Level Aircraft Requirements (TLARs) for our reference airplane

TLAR	Value
Number of passengers	300
Wing aspect ratio	9.3
Number of engines	4
By-pass-ratio	6.5
Range	6,620 NM
Cruise altitude	35,000 ft
Cruise Mach	0.82

Table 3. Key figures describing the reference airplane.

Key figures	Value
Fuselage length	62.8 m
Fuselage diameter	5.64 m
Wing span	58 m
Wing area	361.6 m^2
MTOW	276,500 kg
MZFW	183,000 kg
MLW	192,000 kg
Max fuel weight	113,000 kg
Sea Level Standard Thrust (SLST)	34,000 lb

American Institute of Aeronautics and Astronautics

VI. Propagation of the uncertainties

In this section, we identify the statistical distribution of costs due to the temperature and the airspeed uncertainties by propagating them through the cost module of the process and for the reference airplane presented in Section V. We focus on these two parameters as their distributions were well modeled by the beta distribution function. We therefore consider the airplane as is, but being operated on flights where the parameters are uncertain and follow the distributions presented in Section IV. In this preliminary study, we consider that the uncertainty related to temperature is independent of the airspeed.

The cost that is analyzed is the COC. In order to be able to make comparison between the results and taking into account the fact that the range may vary, we choose to present the COC per passenger and per nautical mile (noted COC/NM/pax, and referred to simply as cost in the sequel).

As a first step in this analysis, we make a screening of the evolution of the cost as a function of the two flight parameters studied and over the scale covered by their distributions. The identification of the statistical distribution of costs is then performed using first- or second-order Taylor-series expansions and moment propagation (MP) techniques. For the sake of this propagation, the first four moments of the temperature and the airspeed are presented in Table 4, together with their skewness and kurtosis.

Both skewness show left-tail distribution features, as illustrated by Figure 11(a) and Figure 13(a). A comparison of the kurtosis reveals that the temperature distribution is slightly less peacky and the airspeed slightly more peaky than the Gaussian distribution function.

In parallel and in order to validate the results, we first perform Monte Carlo Simulation (MCS) and we finally compare the distributions obtained as well as their first four moments.

Table 4. First four moments of the beta distribution for the delta ISA temperature and the cruise airspeed parameters.

	Delta ISA temperature (K)	Cruise airspeed (m/s)
Mean (first moment)	5.03	243.38
Variance (second centered moment)	22.689	15.614
Third centered moment	-23.550	-27.157
Fourth centered moment	1497.1	743.91
Skewness	-0.2179	-0.4402
Kurtosis	2.908	3.0515

A. Delta ISA temperature uncertainty propagation

We first make a screening of the evolution of the cost as a function of the delta ISA temperature. The results are presented with the black curve on Figure 10. The COC increases when the temperature increases, by 1 percent for each 10-degree variation. This is mainly due to the fact that the engine efficiency reduces with higher temperatures. The linearity of this evolution over the range of the temperatures considered brings us to rely on a first-order Taylor-series expansion to propagate the moments presented in Table 4.

Let f_T be the function shown on Figure 10 (in black).

$$\begin{aligned} f_T: \quad \mathbb{R} \quad &\to \quad \mathbb{R} \\ X \quad &\mapsto \quad Y = f_T(X) \end{aligned} \tag{5}$$

where Y is the cost (COC/NM/pax) and X is the uncertain delta ISA temperature. The latter can be expressed as:

$$X = X_0 + Z \tag{6}$$

American Institute of Aeronautics and Astronautics

where Z is a univariate and centered random variable following the beta probability density function associated to the delta ISA temperature and $X_0 = E(X)$ is a constant equal to the X mean value.

The first-order Taylor-series approximation of f_T around X_0 can be expressed as follows:

$$Y = f_T(E(X)) + \frac{df_T}{dX}(E(X))\,Z \qquad (7)$$

It is plotted in red on Figure 10. Based on these notations, the first four moments of the distribution of Y are given by the following expressions :
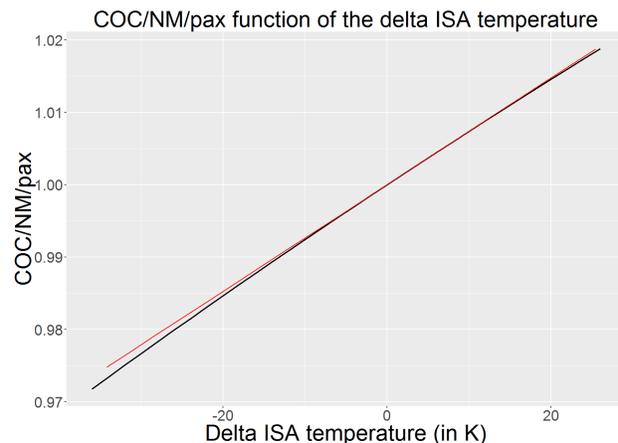
$$
\begin{aligned}
E(Y) &= f_T(E(X)) & (8) \\
Var(Y) &= (f_T(E(X)))^2\,Var(Z) & (9) \\
\mu_3(Y) &= (f_T(E(X)))^3\,E(Z^3) & (10) \\
\mu_4(Y) &= (f_T(E(X)))^4\,E(Z^4) & (11)
\end{aligned}
$$

After calculations, the first four moments obtained for the cost distribution due to temperature uncertainty using MP are given in table 5.

COC/NM/pax function of the delta ISA temperature

Figure 10. Evolution of the COC/NM/pax as a function of the delta ISA temperature (black) and its first-order approximation (red).

The next step of the analysis is to validate this result by comparing it to the distribution obtained using a MCS. A batch of 10^6 random temperature samples is generated from the temperature beta distribution, and the cost associated to each sample is calculated. The calculation time for each sample is around 1 second. In order to reduce the calculation time, we use the response function f_T as a surrogate model. We finally calculate the first four moments from the distribution obtained, and compare them with the output of the MP method. Figure 11 illustrates the input (a) and output (b) distributions for MCS, and table 5 shows the first four moments calculated from the cost distribution.

Table 5. Four-first moments of the beta distribution for the costs due to delta ISA temperature parameter.

Moments	Cost distribution by MP	Cost distribution by MCS	Relative difference
$E(Y)$	1.0037	1.0037	0.0 %
$Var(Y)$	1.234e-5	1.239e-05	0.4%
Third centered moment	-9.456e-09	-10.720e-09	13.4%
Forth centered moment	4.435e-10	4.488e-10	1.2%

This sub-section has shown that the propagation of the uncertainty related to the temperature based on the moment propagation method is valid. In the next section, we focus on the uncertainty propagation for the airspeed.

B. Airspeed

We follow the same method as described above. The screening is realized and the evolution of the cost with respect to the airspeed variability is presented with the black curve in Figure 12. The cost increases when the airspeed increases. This is related to the effect of the Mach number on the aerodynamic efficiency of the airplane and more precisely the compressibility effects. When speed reduces, the cost finds a minimum before increasing again. This is related to the existence of an optimum speed for each altitude. Since this curve is not linear, we rely on a second-order Taylor-series expansion to propagate the moments of the airspeed uncertainty beta distribution.

Let f_{AS} be the function shown on Figure 12 (black):

$$
\begin{aligned}
f_{AS}: \quad \mathbb{R} &\rightarrow \mathbb{R} \\
X &\mapsto Y = f_{AS}(X)
\end{aligned}
\qquad (12)
$$

American Institute of Aeronautics and Astronautics

where Y is the cost (COC/NM/pax) and X is the uncertain airspeed. It can be expressed, as in Section VI.A:

$$X = X_0 + Z \tag{13}$$

where Z is a univariate and centered random variable following the beta probability density function associated to the airspeed and $X_0 = E(X)$ is a constant equal to the X mean value.

The second-order Taylor-series expansion of this function around X_0 is:

$$Y = f_{AS}(E(X)) + \frac{df_{AS}}{dX}(E(X))Z + \frac{1}{2}\frac{d^2 f_{AS}}{dX^2}(E(X))Z^2 \tag{14}$$

The approximation is plotted in red in Figure 12.

In order to calculate the four first moments of the distribution of Y, and to simplify the equations, we set the following notations :

$$a = \frac{df_{AS}}{dX}(E(X)) \tag{15}$$

$$b = \frac{1}{2}\frac{d^2 f_{AS}}{dX^2}(E(X)) \tag{16}$$

The two first moments are then expressed by the following equations:

$$E(Y) = f_{AS}(E(X)) + bE(Z^2) \tag{17}$$

$$Var(Y) = a^2 E(Z^2) + 2abE(Z^3) + b^2 E(Z^4) - b^2 E(Z^2)^2 \tag{18}$$

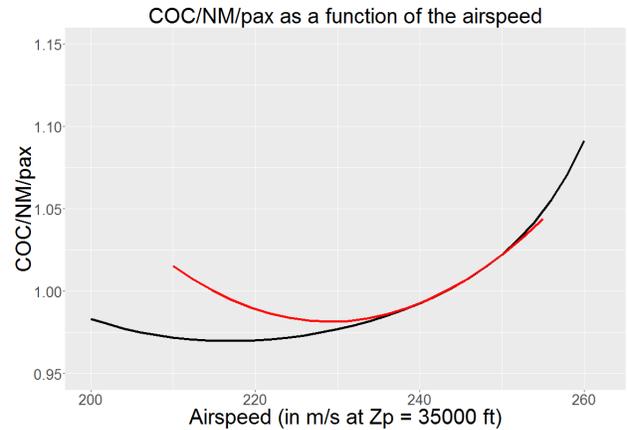The third and forth moments are not presented here because of their complexity.

The results of the calculation are presented in the first column of table 6. We compare them with two other results, obtained by MCS. The sample size used for the MCS is 10^7. Again, to speed up the process, the response function f_{AS} is used as a surrogate model.

The first MCS is based on the second-order Taylor-series expansion presented in eq. 14 and . This first comparison permits to evaluate how efficient the MP is in this case. We can see a very good matching with the MP results.

The second comparison is made with the results of the MCS based on OCCAM response function f_{AS}. This second comparison quantifies the overall accuracy of the method. A good matching is observed. The differences seem to be explained by the fact that the Taylor-series expansion used reaches its minimum in the interval where the input beta distribution is bounded, although f_{AS} is monotonic on this interval.

Figure 12. Evolution of the COC/NM/pax as a function of the airspeed (black) and its 2nd-order approximation (red).

Concerning the skewness, we observe that the three simulations exhibit right-tailed output distributions. Finally, comparing the kurtosis reveals that they produced distributions flatter than the Gaussian distribution function.

Figure 13(a) shows the airspeed distribution used as input for the MCS. The three distributions that were obtained from simulations are displayed on Figure 13(b): the MP distribution is represented by the red curve, while the MCS results are plotted as histograms. The red histogram corresponds to the MCS based on the OCCAM response function f_{AS}, and the blue histogram represents the MCS based on the second-order Taylor-series expansion. These three distributions exhibit a good matching. The left tail of

American Institute of Aeronautics and Astronautics

Table 6. First four moments of the beta distribution for the costs due to airspeed parameter.

Moments	MP	MCS with Taylor[*]	Relative difference	MCS with OCCAM[+]	Relative difference
$E(Y)$	1.0020	1.0019	-0.01 %	1.0018	-0.02 %
$Var(Y)$	1.0086e-5	1.0090e-05	0.05 %	1.0466e-05	-3.63 %
Third centered moment	2.928e-07	2.934e-07	0.23 %	2.381e-07	23.0 %
Forth centered moment	2.605e-08	2.607e-08	0.07 %	2.996e-08	-13.1 %
Skewness	0.289	0.289	N/A	0.222	N/A
Kurtosis	2.561	2.560	N/A	2.736	N/A

[*] MCS realized using the second-order Taylor-serie expansion presented in eq. 14.

[+] MCS realized using the OCCAM model.

the blue distribution is cut. This is due to the fact that the Taylor expansion reaches its minimum in the interval where the airspeed distribution is bounded.

This sub-section has shown that MP techniques are very efficient for determining the cost distribution arising from airspeed variability. We have compared MP results with those produced using two MCS strategies, one relying on the actual OCCAM response function, and the other one based on the second-order Taylor-series expansion. In both case, differences appear to be negligible.

VII. Conclusion

The aim of this paper was to model airplane operational parameter uncertainties in order to quantify the resulting uncertainty in the estimation of the cost of the mission. The four flight parameters considered were the air range, the average cruise altitude, the average cruise speed and the average difference between the air temperature in cruise and the ISA temperature at the same altitude. The cost observed was the cash operating cost per nautical mile per passenger. The data were extracted from the MOZAIC database. We then focused our analysis on four particular airplanes of one specific long-range type. The model chosen for building the associated statistical distribution was a beta distribution. It proved to be efficient to model airspeed and temperature distributions but not for air range and cruise speed. We therefore focused on these first two parameters and propagated them to identify the related distribution of operational costs. A first-order Taylor-series expansion combined with the moment propagation technique was used for the temperature and yield good results. A second-order Taylor-series expansion together with moment propagation was used for the airspeed and the results validated the method used.

Concerning the impact on cost, we showed in the preliminary analysis that the effect of air range could be high. For airspeed and temperature, the variability observed is much smaller and of one order of magnitude of few percents.

In this work, we have used a tool dedicated to overall airplane preliminary design, and the propagation of the studied uncertainties can be propagated and later used for robust design optimization in order to meet better the needs of the airlines and the passengers, and to limit the human impact on the environment through more efficient design and operation interconnections.

Further work is now anticipated to push the limit of the presented analysis. First, in this paper, only the average values during cruise were considered for altitude, speed and temperature, although much more data is available from the database. Also, these parameters have been considered to be independent although inter-correlations between them probably exist. Payload is another important parameter that has not been included in our analysis because it was not available. We also limited our study to beta distributions for representing the operational variabilities. Other statistical models should be considered to grasp furthermore information from the data available. We limited the study to the costs but it could be broaden to other parameters of interest (mass, etc.).

American Institute of Aeronautics and Astronautics

Acknowledgments

References

[1]ACARE, "Strategic Research and Innovation Agenda," http://www.acare4europe.com/sria, 2012, Advisory Council for Aviation Research and innovation in Europe.

[2]OAG, "OAG Analyser/Schedules Analyser," http://analytics.oag.com, 2015, OAG Aviation Worldwide Ltd.

[3]IAGOS, "MOZAIC IAGOS Database," http://www.iagos.org/, 2016, European Research Infrastructure IAGOS (In-service Aircraft of a Global Observing System).

[4]Birman, J., *Uncertainty quantification and propagation in Conceptual Aircraft Design: From deterministic optimization to chance constrained optimization*, Ph.D. thesis, Université de Toulouse III - Paul Sabatier, Toulouse, France, 2013.

[5]Prigent, S., *Innovative and integrated approach for environmentally efficient aircraft design and operations*, Ph.D. thesis, ISAE-Supaero, Toulouse, France, 2015.

[6]"Scilab," http://www.scilab.org/, 2016, Scilab Enterprises S.A.S.

[7]Lambe, A. B. and Martins, J. R. R. A., "Extensions to the design structure matrix for the description of multidisciplinary design, analysis, and optimization processes," *Structural and Multidisciplinary Optimization*, Vol. 46, No. 2, 2012, pp. 273–284.
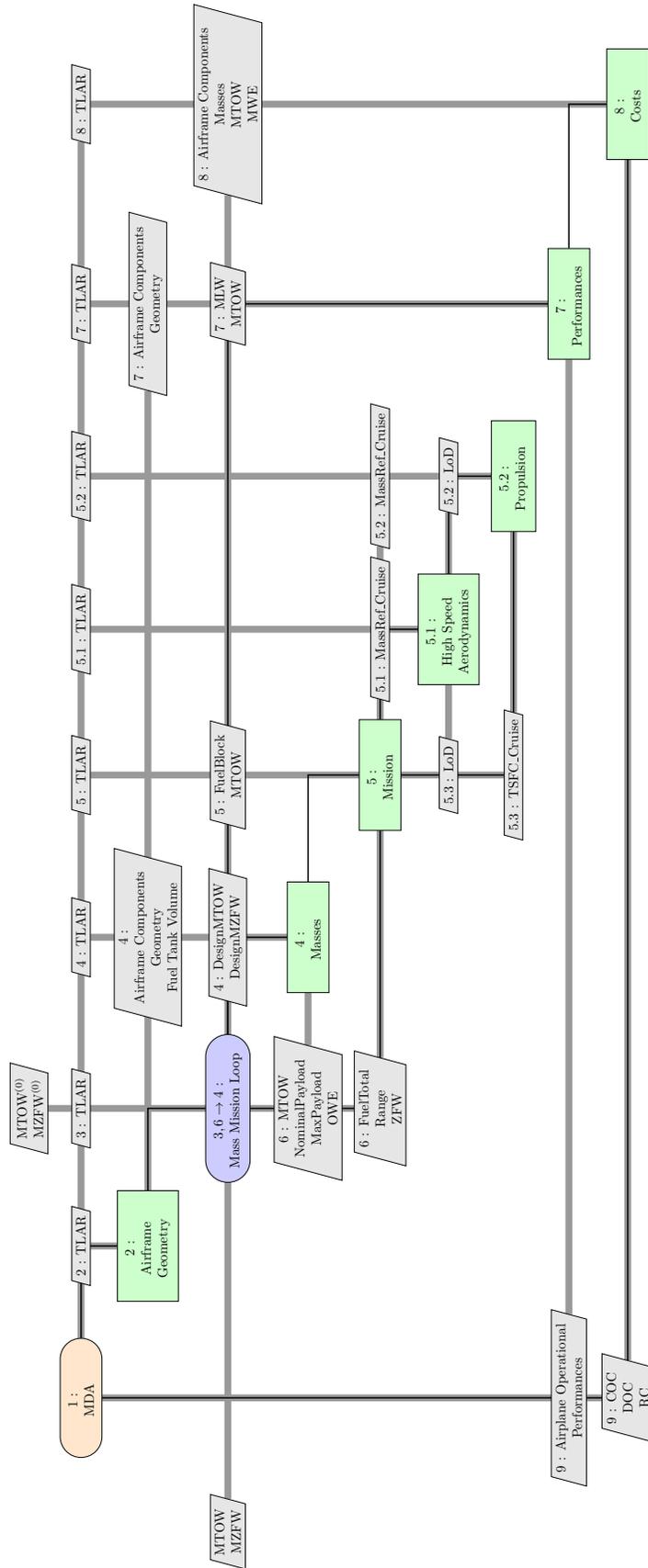
Figure 8. Multidisciplinary Design Analysis Process used for the propagation of the uncertainties
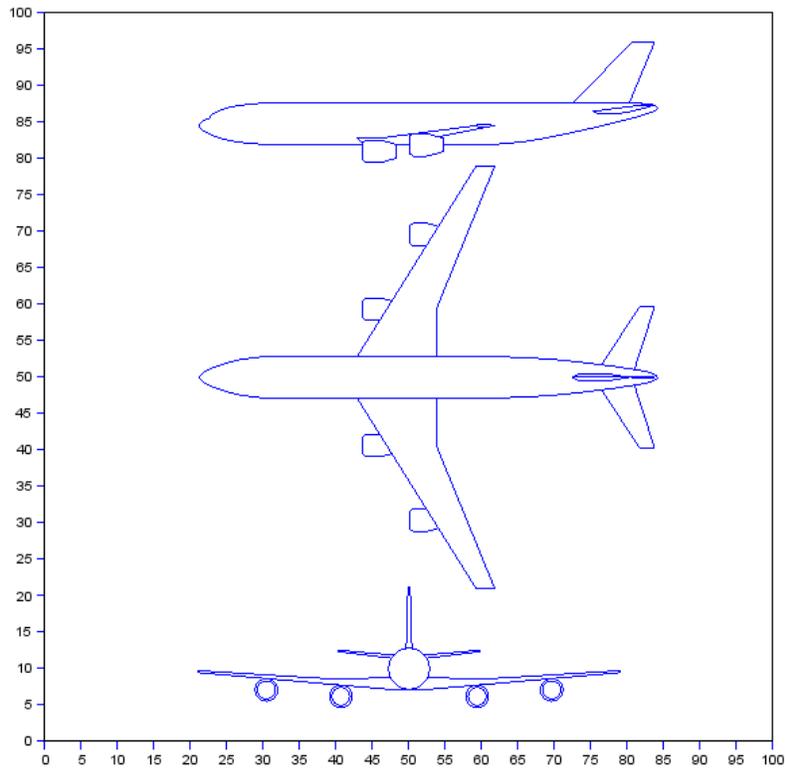
American Institute of Aeronautics and Astronautics
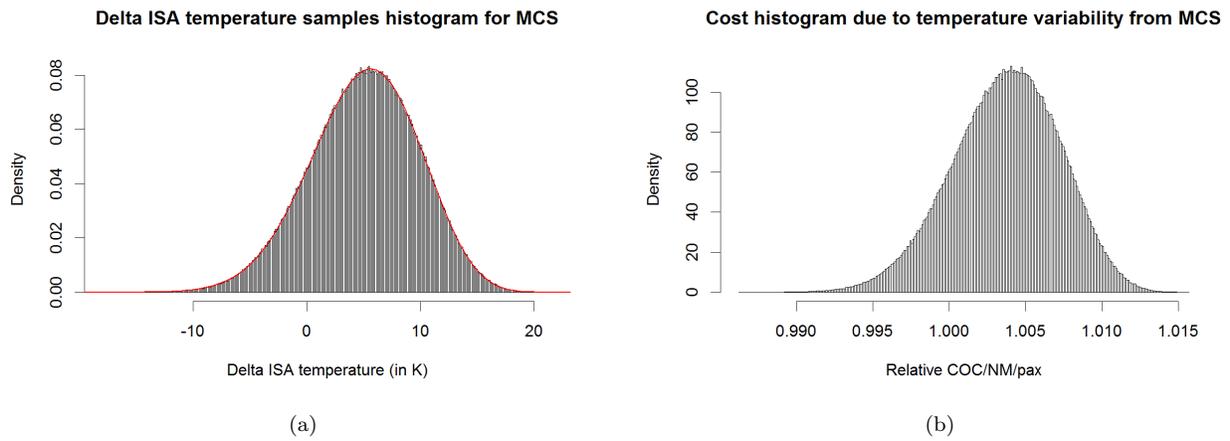
Figure 9.   3-view drawing of the reference airplane.

(a)

(b)

Figure 11.   Monte Carlo simulation input and output distributions for delta ISA temperature variability

American Institute of Aeronautics and Astronautics
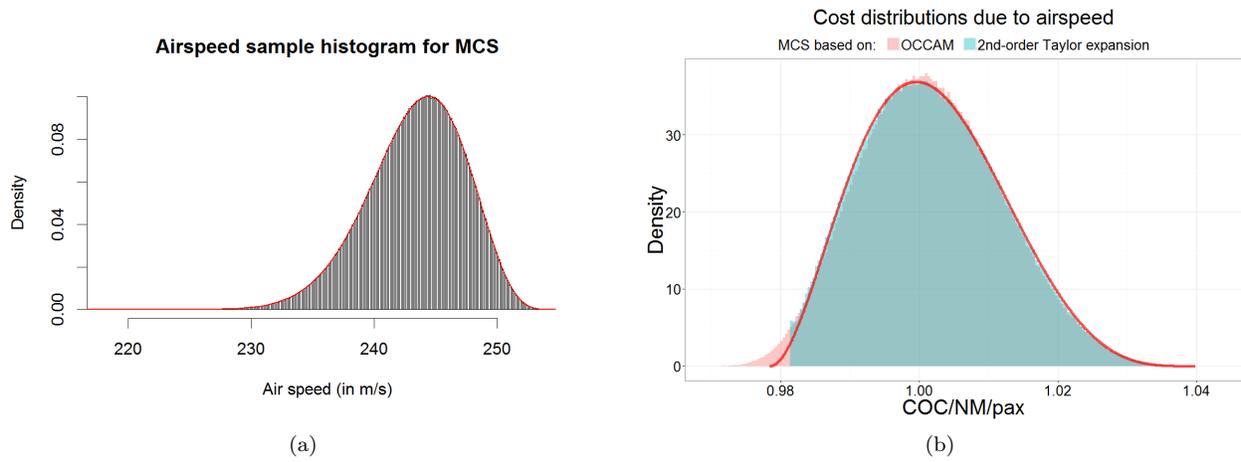
(a)

(b)

Figure 13. **Monte Carlo simulation input and output distributions for airspeed variability**